

NUMERICAL INVESTIGATION OF SHOCKWAVE TURBULENT BOUNDARY LAYER INTERACTION AT MACH 2.5 OVER A COMPRESSION RAMP

Sreenika Gunasekaran[1], Zeeshan A. Rana[2] & Simon Prince[1]

[1]School of Aerospace, Transport and Manufacturing, Cranfield University, UK, MK43 0AL
[2]Department of Mechanical Engineering, Prince Mohammad Bin Fahd University, Al-Khobar, KSA

Abstract

A canonical shockwave-boundary layer interaction experiment is planned in a small working section supersonic wind tunnel, that will allow detailed measurements of the effects of various surface treatments, such as sand grain roughness, to be acquired to allow for tuning of high fidelity CFD methods. This paper presents preliminary results of a steady CFD campaign to support the design of the experiments, involving the Mach 2.5 flow past a compression ramp to understand the 3D flow behavior in the tunnel test section. The investigation covered various ramp angles and distinct flow regimes, including fully attached flow, small separation bubble and large separation bubble. The pressure distribution over the ramp was examined to determine the positions of the separation and reattachment fronts which will be 3D in nature, in comparison with the purely 2D case. Computational results from Reynolds-averaged Navier-Stokes (RANS) were compared with theoretical solutions. The predicted upstream movement of the separation line on the flat plate, and the downstream movement of the reattachment line on the ramp, allows for the proper placement of the kulite surface pressure sensors for the experimental campaign.

Keywords: Hypersonic Flow, Turbulent Flow, Boundary Layer, Compression Ramp, Shockwaves

1. Introduction

Shockwave boundary layer interactions (SWBLI) are complex and fascinating phenomena that demand our attention in fluid dynamics and aerospace engineering which are considered as common features in high-speed flows. In practical scenarios, such interactions manifest on the transonic wings of civil aeroplanes, supersonic inlets, control surfaces of high-speed aircraft, missile base flows, reaction control jets and over expanded nozzles. The SWBLI over a compression ramp serves as a simplified representation of the various interactions over deflected control surfaces[1]. Hence, understanding SWBLIs require an introduction to the physics of shock waves and boundary layers, along with an exploration of the complexities inherent and the strategies for managing such phenomenon.

In examining the SWBLIs at M=2.5, several ramp angles were chosen to facilitate a detailed flow visualization and data analysis. A zero degree ramp angle was selected to get the baseline experimental data. Then, angles ranging from 13° to 27° were explored as a separation bubble typically started to occur between 12° and approximately 28° [2]. While existing research primarily addresses ramp angles up to about 30°, angles exceeding 30° were also included for comprehensive analysis [3]. Table 1 indicates the chosen ramp angle for each run. Starting from the third run, the ramp angle was determined by analysing the Schlieren image from the preceding run and may differ from the initial selection.

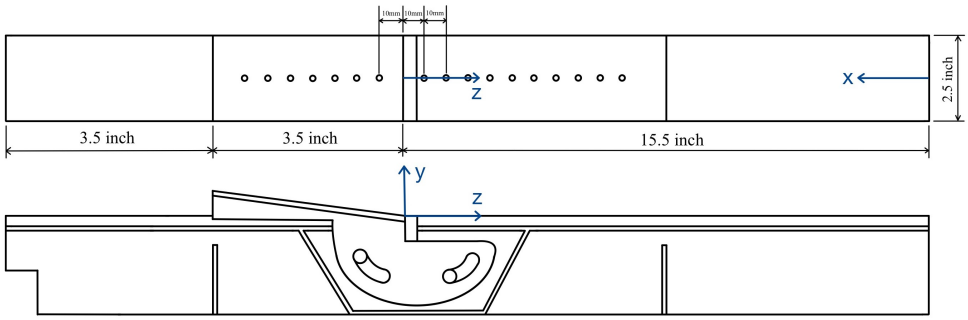


Figure 1 – Schematic diagram of compression ramp

Table 1 – Test cases for initial selection

Run No.	**1**							**2**						
Ramp angle	0	5	10	13	16	19	22	25	28	30	32	34	36	38

The computational study was done for similar angles and was compared with the experimental results. RANS was conducted for all the ramp angles whereas DES was carried out for certain specific angles where the flow had small separation bubble and large separation bubble.
When SWBLIs occur, the increase in shock pressure creates an adverse pressure gradient on the approaching boundary layer, which can thicken the boundary layer and may even cause separation, thus amplifying the viscous dissipation within the flow[1]. The impact on flow applications due to this problem can be severe; therefore, research in flow fields characterized by SWBLIs has been nonstop for the last few decades to eliminate these negative effects through a better understanding of the physics behind these.

1.1 Compression Corner Interaction

In the compression corner scenario, the geometry dictates the primary flow deflection, with both the attached and separated flow fields exhibiting a common characteristic that is compression waves generated by streamline curvature merge into a far-field shock, causing a single pressure rise of roughly one boundary layer thickness [4]. As numerous simulations and experiments were carried out, it was found that separation invariably occurs regardless of the ramp angle and that the size of the separation bubble can be seen as the boundary between small and large-scale separation [5]. Hence, the difficulty of defining the relationship between the separation point and the ramp angle then arises [6]. To solve this problem, the technique of measuring the smallest separation size can therefore define the separation point [7]. According to the measurement technique, as the ramp angle

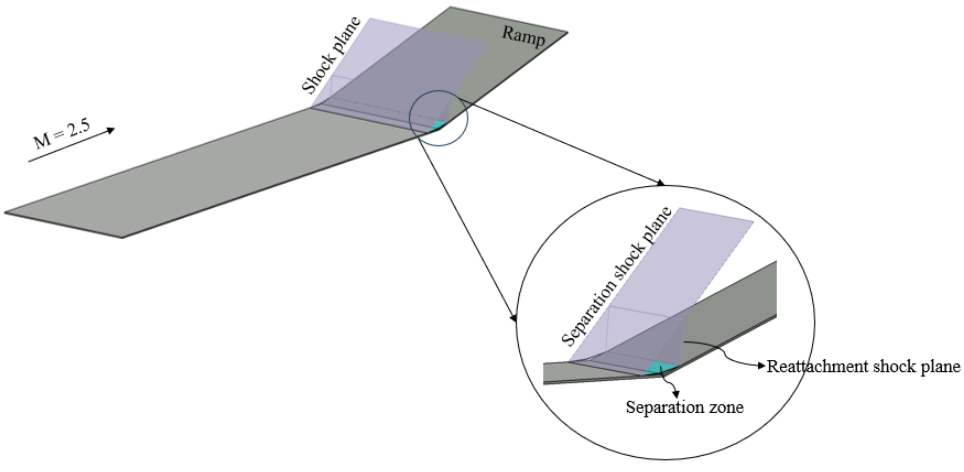


Figure 2 – Schematic diagram of SWBLI over compression ramp

increases, five distinct regimes emerge: absence of measurable separation; irregular occurrence of small-scale separation; gradual growth of separation length with deflection angle; sudden escalation in separation length scale with increasing deflection angle; and lastly, for significant deflection, the expansion fan at the end of the finite [8].

1.2 Two-dimensional SWBLI Theory

To unravel the fundamental flow phenomena of SWBLIs, researchers primarily simplified investigations by focusing on two-dimensional (2D) configurations. These interactions commonly fall into one of three categories: the normal shock interaction, the impinging oblique shock reflection, and the compression corner interaction [9]. Each of these interactions displays unique wave patterns and underlies disparities influenced by the attachment or separation of the boundary layer.

1.3 Three-dimensional SWBLI Geometries

Initially, studies focused on simpler two-dimensional problems. Now, with a better under-standing of the involved processes from these studies, attention is shifting towards tackling the interaction problem in three dimensions (3D). Various canonical geometries are relevant in high-speed aircraft applications. However, when considering the swept compression corner and the sharp unswept fin, the theory describing 2D SWBLI is applicable in these scenarios [9] The first exploration of 3D interactions delved into experiments concerning the inter-action of turbulent boundary layers and shock waves with sweptback configurations, which revealed that for moderate sweep angles, the peak pressure rises at separation, the upstream influence ahead of separation, and the pressure rises at reattachment can all be comprehended through straightforward extensions of existing two-dimensional theories [10]. Later on, Settles and Dolling [11] as well as Smits and Bogdonoff [12] subsequently offered an in-depth review of three-dimensional interactions, underscoring the significance of advancing experimental methodology. With the continual evolution of experimental methods, Panaras [13] used non-intrusive experimental methods and proved many hypotheses posited by early researchers were in fact correct. Fast forward to the present, Zheltovodov and Knight [14] have leveraged advancements in simulation technology to provide further insights into 3D interactions. As both experimental and computational technologies evolve, further discoveries continue to emerge.

1.4 Effect of Ramp Deflection

In 2020, Zhengzhong [15] visualized the effect of ramp using schlieren method and concluded that by increasing the ramp angle, the turbulent region over the surface becomes thick and the separation bubble gradually moves upstream which further separates the two shock waves. The surface pressure distribution over the ramp also increases as ramp angle increases. The reattachment shock gets stronger over large compression ramp whereas the ramp deflection does not affect much on separation shock waves[16]. The interaction between the boundary layer and shock wave results in a near-wall region post-separation shock wave exhibiting significantly stronger compared to the incoming turbulent boundary layer. This can induce pulsations in bubbles, triggered by a global instability prompting fluctuations in the reattachment point. These fluctuations in the reattachment point lead to expansions/contractions of the bubble and coordinated movement of the separation line, separation shock (outside the boundary layer), and separation shock foot [17]. For smaller ramp angle, the intermittent region and mean separation location are formed closer to the apex [18].

1.5 Effect of shock strength

The shock strength is characterized by the pressure increase across the shock wave increases as ramp angle increases [18]. The corner flows are influenced by shock strength [19]. At weaker shock strength, it is easy to predict a channel of attached flow between the sidewall and center line separation whereas in the presence of strong strength, the channel of attached flow disappears but provide the maximum turbulence intensity that occur further from the ramp surface [2]. This paper presents a computational study of shockwave-boundary layer interactions (SWBLI) using the SST $k-\omega$ turbulence model over a two-dimensional compression ramp. The results are compared with analytical solutions for validation. Ramp angles (β) of 6°, 9°, 12°, 15°, 18°, and 21° were considered for further

analysis.

A shock wave arises as a propagating disturbance in a medium that carries energy which will form when a source exceeds the speed of sound. In the air, molecules within a supersonic flow will collide with each other when a shock passes, and experience significant deceleration at the wavefront, which at now the thickness of a shock front is only a few molecular mean flow paths. Therefore, a shock wave can be envisioned as a wall of compressed, hot gas travelling through the medium at supersonic speeds.

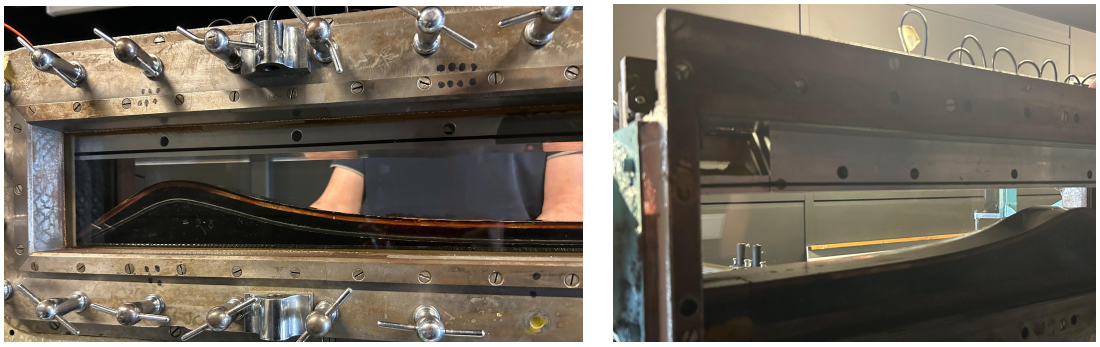


Figure 3 – Test section in the wind tunnel

A boundary layer refers to a thin region of flow near a solid surface, transitioning from the surface's velocity to that of the free stream, forming as a result of friction between the fluid and the surface. As fluid flows over a surface, molecules in direct contact experience deceleration due to viscosity, creating a velocity profile from zero at the surface to nearly the free stream velocity at the edge of the boundary layer. The behaviour of the boundary layer significantly affects the overall flow characteristics. Two distinct flow characteristics are identified in the boundary layer: the laminar boundary layer and the turbulent boundary layer. These differ in that the turbulent boundary layer has a much "fuller" profile with a more complex structure and can sustain this structure for a longer duration than the laminar boundary layer when subjected to a significant pressure gradient.

In basic SBLIs within two-dimensional (2D) flows, five types of interactions are observed: an impinging oblique-shock reflection, a ramp flow, a normal shock, an imposed pressure jump, and an oblique shock induced by a forward-facing step [1]. As a shock invades to or originates from a boundary layer, it travels through the viscous and inviscid flow structure within the boundary layer, subsequently imposing an adverse pressure gradient. This leads to the thickening of the boundary layer and potentially induces separation. When the shock is sufficiently strong to induce boundary layer separation, it introduces flow unsteadiness [20].

The challenges encountered in the development of high-speed vehicles and propulsion systems underscore the significant impact SBLIs can have on their performance and, crucially, on human safety. For instance, in civil aeroplanes operating at transonic speeds, flow instabilities and buffeting on the wings can significantly increase drag and potentially cause structural damage. Similarly, engine intakes in supersonic and hypersonic flows can create a chaotic flow to the compressor therefore an increase in the internal flow losses. For launch and re-entry vehicles, flow instabilities can pose significant control challenges and cause peak thermomechanical loads at the surface [21]. As the shock waves in these situations get strong enough, the occurrence of flow separation will result in generating intense vortices or complex shock patterns, which may trigger shock oscillations. There-fore, these complications highlight the importance of addressing SBLIs in high-speed vehicle design and operation [22].

2. Methodology

2.1 Flow configuration and boundary condition

The flow domain was designed to replicate the experimental setup conducted in the supersonic wind tunnel at Cranfield University with a test section of 0.572m $\times$ 0.0635m. The model features a compression ramp mounted over the flat plate in the post region of the throat section. The 2D geometry used in the simulation spans from 0 to 0.35m along the flow direction (X-direction). In the direction normal to the flat plate (Y-direction), the domain extends to 0.0635m. The hinge point where the flat plate is connected to the ramp is positioned at ξ = 0.211m. The boundary conditions for the 2D internal domain configuration are illustrated in the figure 4. Since the outlet pressure was unknown, a minimum pressure of 1 Pa was imposed for back-flow in the outlet zone.

Table 2 – Inflow conditions

Freestream flow properties	Value
Mach number	2.5
Total Pressure (Pa)	101325
Total Temperature (K)	288.1
Static Pressure (Pa)	5930.3
Temperature (K)	127.9
Reynolds number based on L	3.6e+06

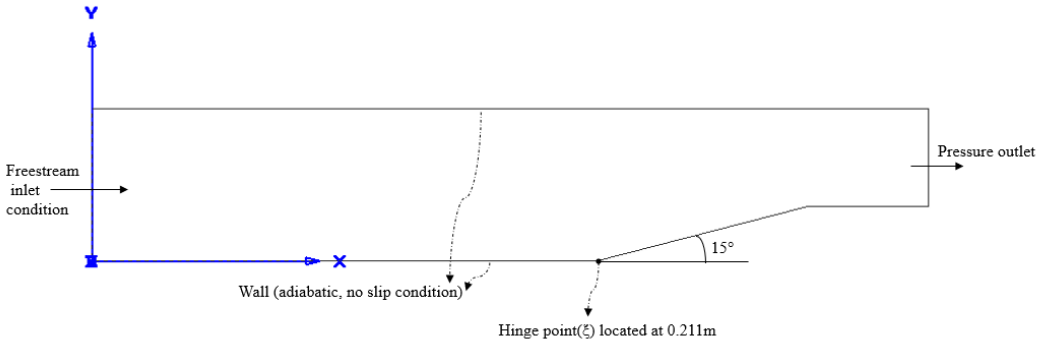


Figure 4 – Sketch of the 2D computational domain

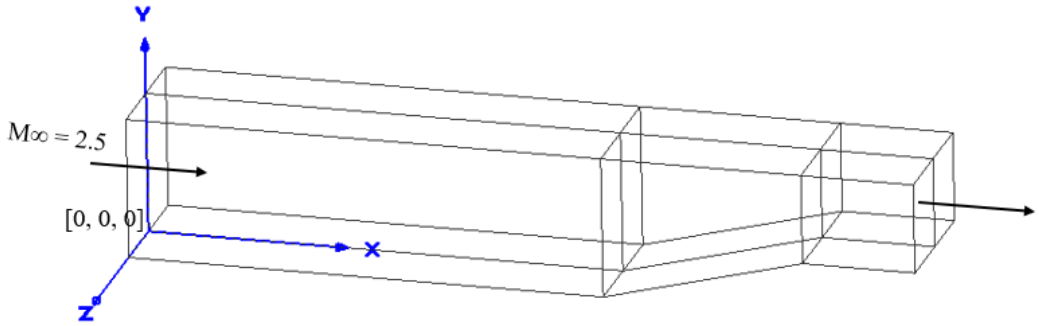


Figure 5 – Sketch of the 3D computational domain

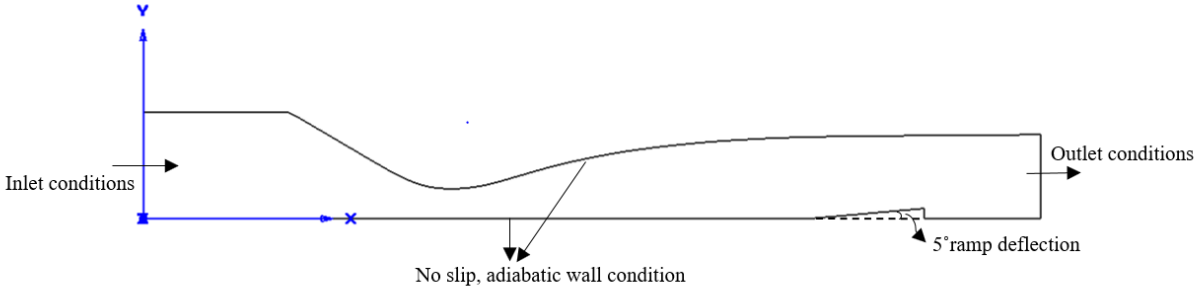
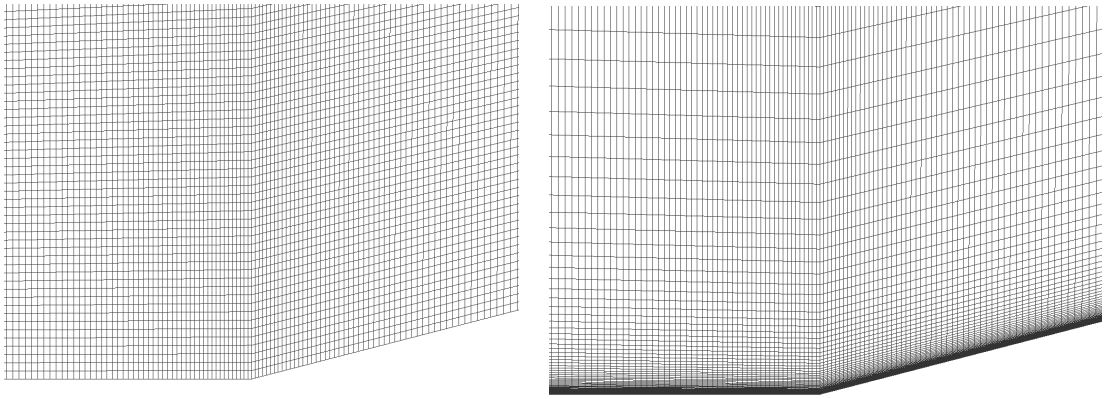


Figure 6 – Sketch of the computational domain for DES model

For the 3D structure, the geometry of two dimension was stretched from the origin at z=0 plane in the direction [-0.03175, 0.03175]m as shown in the figure 5. In the normal direction of the flow, the domain expands in the positive y-axis up to 0.0635m. The length of the domain is maintained the same as the 2D length, which was 0.35m. Non-slip, adiabatic wall boundary condition was used for the side walls. The table 2 presents the freestream flow properties used as the inflow conditions for the numerical investigation.

The model features a compression ramp placed over a flat plate, positioned on the top wall of the test section. The test section includes a throat section to accelerate the flow to supersonic speed. The inlet condition were freestream total temperature T_o = 288.15K and freestream total pressure P_o = 10^5Pa corresponding to a freestream Reynolds number R_e = 3.6 $\times$ 10^6. By trial and error method, the inlet Mach number was assumed as M_i = 0.5 with a calculated back pressure of 0.6 $\times$ 10^5Pa to obtain a flow velocity of 850m/s at downstream of the throat section. The diagram in Fig. 6 illustrates the computational flow domain and the corresponding boundary conditions utilized for the DES model.



(a) 2D mesh (b) 2D mesh with y^+ = 2 near the ramp

Figure 7 – Structured mesh on 2D domain (β = 15°)

2.2 Mesh generation

A structured mesh was generated with 100K, 200K and 400K cells, providing enhanced control and refinement near the compression corner region. A Grid Convergence Index (GCI) study was performed between the coarse, medium, and fine meshes to verify the accuracy and reliability of the simulation results by evaluating the impact of mesh refinement on the solution. Figure 7 presents the evolution of the 2D mesh generation. The mesh quality was determined by various elements like skewness, smoothness (i,j), aspect ratio and orthogonality. The constructed mesh under study has a maximum skewness of 0.29. Similar meshes were generated for other ramp angles. The primary objective of this study was to accurately capture the separation region, leading to mesh refinement

near the wall with y-plus values of 4, 2, and 1 for the coarse, medium, and fine meshes, respectively.

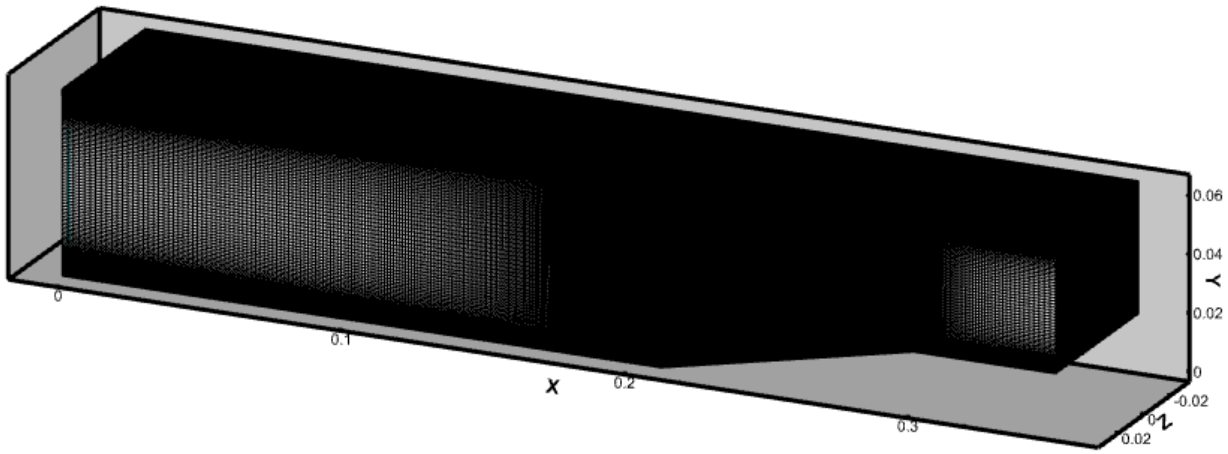


Figure 8 – Structured mesh on 3D domain (β = 15°)

The Grid Convergence Index (GCI) study was conducted to compare the simulation results with the theoretical values of post-shock pressure and Mach number. The medium mesh, consisting of 750x285 cells with y^+ = 2 (wall distance of 5e-06m), offers a strong correlation with the theoretical values while balancing computational cost and time. For 3D domain, a structured mesh was utilised, comprising 20 million cells. Figure 8 depicts the mesh corresponding to a 15°ramp deflection. The mesh was divided into six blocks, achieving an equiangle skewness of 0.16. To accurately capture the separation and reattachment regions, the mesh was refined with y^+ = 2 near the ramp corner and z^+ = 20 along side walls. In STAR-CCM+, the steady boundary conditions were defined as freestream at the inlet, pressure outlet at the exit and non-slip adiabatic wall at the upper and lower surfaces of the domain.

Table 3 – GCI study at β = 15°

Mesh size	P_2/P_1	M_2
Theory	2.468	1.874
100K	2.507	1.8621
200K	2.500	1.865
400K	2.498	1.8683

2.3 Computational setup

In Star CCM+, the initial setup involved a 2D, steady, coupled flow, ideal gas property in a turbulent regime, modeled using the RANS framework with the SST $k-\omega$ turbulence model. The flow was solved using implicit integration with second-order discretization. An automatic CFL (Courant-Friedrichs-Lewy) adjustment was employed, ranging from 0.1 to 1, with an initial value set to 0.5. For the 3D simulations, the setup followed a similar procedure as the 2D configuration, with differences in dimensions and axis definitions. An adaptive mesh refinement based on static pressure was applied on 3D mesh to sharply capture the shock, with cell refinement concentrated along the shock regions. This process was specifically performed for the 9°ramp angle, increasing the cell count from 20 million to 38 million.

From the past numerical finding [23], it was concluded that conventional Reynolds-Averaged Navier-Stokes (RANS) models cannot predict the location of the separation shock, size of the separation region at the corner and mean velocity profiles downstream of the interaction at high deflected ramp

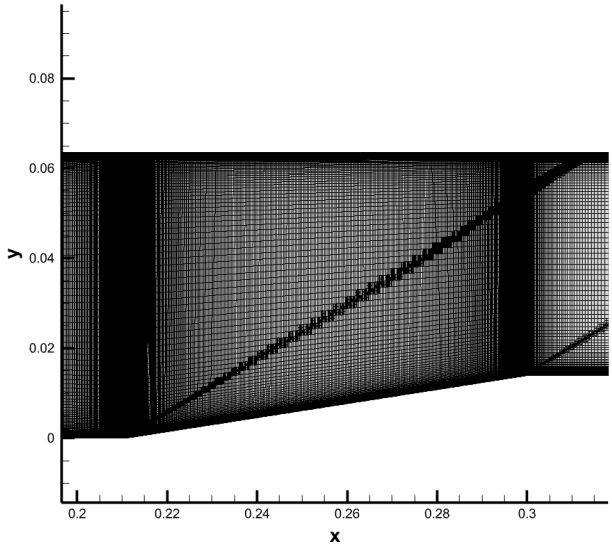


Figure 9 – Adaptive mesh on 3D domain (for $\beta = 9^{\circ}$) to capture the shock sharply

angle of the compression corner. So the converged solution from steady RANS was used as the initial condition for DES models. The Sutherland's law is used to calculate the viscosity co-efficient and the ideal gas state equation is enforced as the flow is supersonic. The third order MUSCL method was employed with AUSM flux type. Setting up DES for complex structures becomes quite easy by creating the necessary journal (jou.) and subject (sub.) files to input in High Performance Computing (HPC).

3. Results and Discussion

The flow properties across the oblique shock (separation shock) from the 2D simulation results were compared with theoretical solutions calculated using oblique shock relations. The 3D results (at the z=0 plane) were then compared to the 2D results to determine whether the 2D CFD analysis could accurately predict the 3D flow in the narrow wind tunnel domain.

3.1 2D analysis

3.1.1 Post-shock flow properties

The post-shock flow properties obtained from the simulation results are compared with the analytical solutions which was obtained from oblique shock relations. In table 5, θ represents the oblique shock

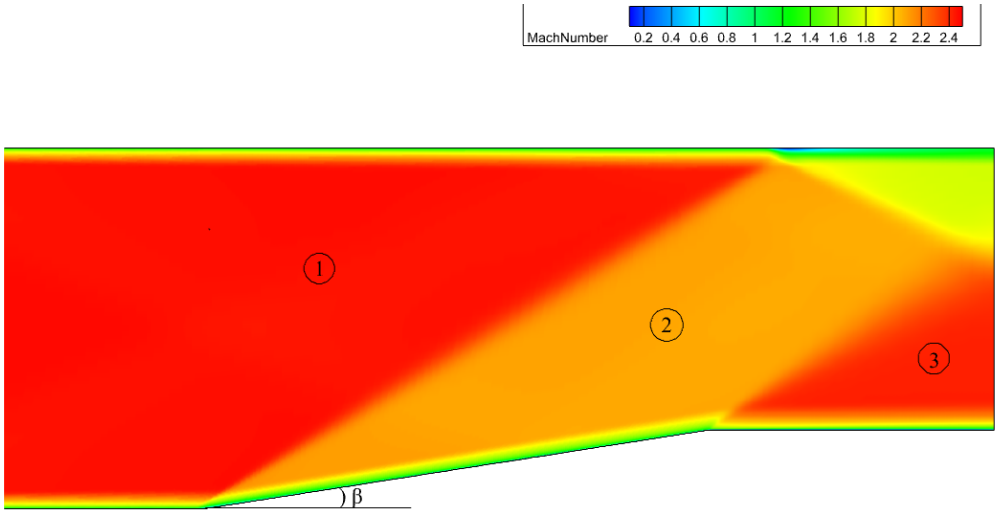


Figure 10 – Stations across the ramp region

angle. The error percentage was minimal when the 2D results were compared with the analytical data, demonstrating strong agreement. This minimal error validates the accuracy of the computational data.

Table 4 – Flow properties across oblique shock wave

β (deg)	Theoretical data		Simulation results		Error %	
	P_2/P_1	M_2	P_2/P_1	M_2	P_2/P_1	M_2
6	1.468	2.250	1.509	2.233	2.793	0.756
9	1.758	2.127	1.827	2.101	3.936	1.222
12	2.090	2.002	2.151	1.984	2.899	0.924
15	2.468	1.874	2.500	1.865	1.317	0.454
18	2.895	1.739	2.936	1.738	1.417	0.040
21	3.379	1.597	3.361	1.619	0.533	1.352

Table 5 – Flow properties across oblique shock region

β (deg)	Theoretical data			Simulation results			Error %		
	T_2/T_1	ρ_2/ρ_1	θ (deg)	T_2/T_1	ρ_2/ρ_1	θ (deg)	T_2/T_1	ρ_2/ρ_1	θ (deg)
6	1.118	1.313	28.260	1.127	1.340	27.617	0.861	2.010	2.274
9	1.181	1.489	30.915	1.196	1.530	30.726	1.245	2.759	0.611
12	1.249	1.674	33.806	1.260	1.708	34.514	0.914	2.024	2.094
15	1.322	1.867	36.945	1.329	1.894	37.255	0.536	1.447	0.839
18	1.402	2.065	40.389	1.403	2.094	39.973	0.120	1.381	1.030
21	1.490	2.268	44.216	1.474	2.283	43.420	1.072	0.633	1.800

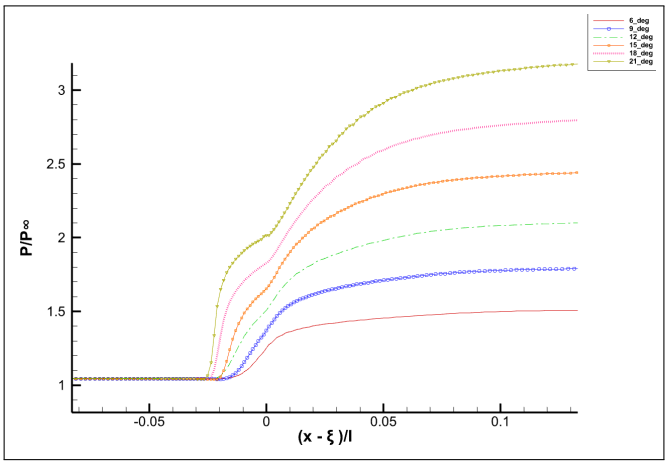


Figure 11 – Pressure distribution over compression ramp

From the figure 11, it can be noticed that before the intersection point ($\xi = 0$), the pressure remains constant and close to the freestream pressure ($P/P_\infty = 1$), indicating that the flow is attached and the boundary layer is developing smoothly without any significant pressure increase. As the flow approaches the intersection point, a noticeable rise in pressure occurs due to the oblique shock wave generated at the ramp, which compresses the flow. The initial inflexion in the pressure plot indicates the onset of separation. The sudden jump in the pressure was observed at the intersection (hinge point). The significant rise in the pressure distribution downstream of the hinge point marks the reattachment location. The pressure distribution on the compression ramp increases as the ramp angle increases, indicating the impact of the shock strength.

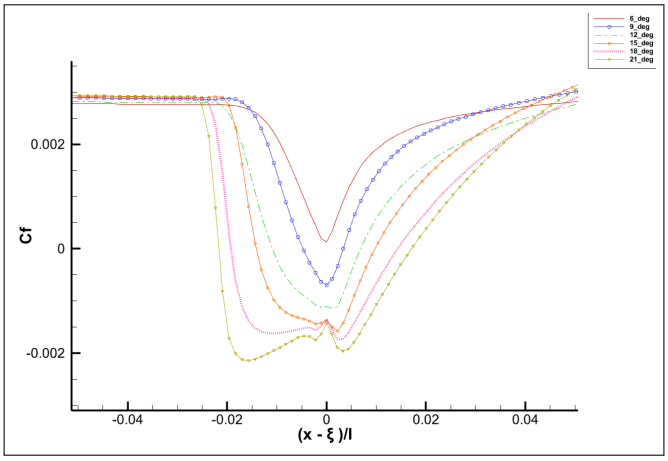


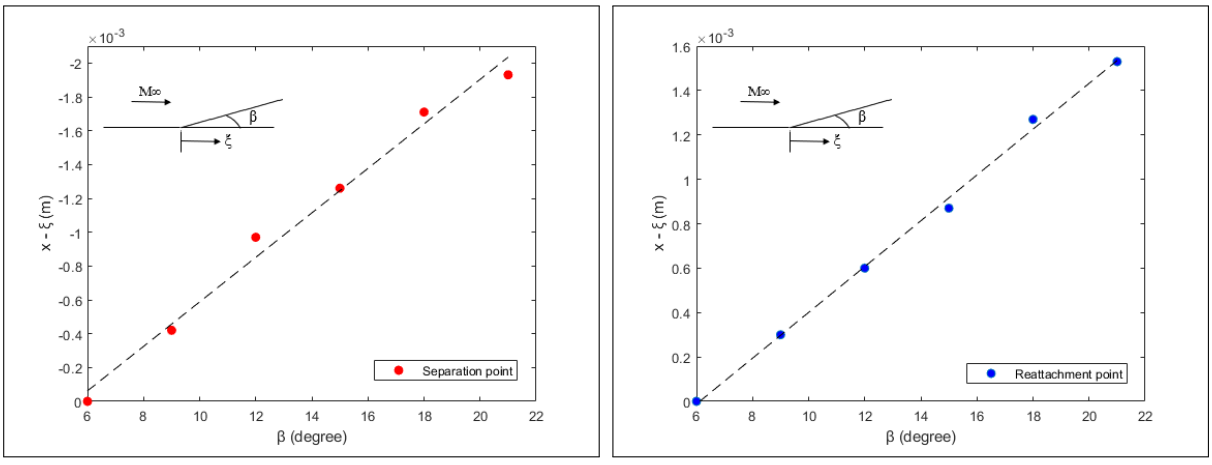
Figure 12 – Skin friction coefficient over compression ramp

3.1.2 Separation and reattachment points

To obtain the exact location of separation/reattachment point, it is necessary to plot the coefficient of friction

$$\left(\frac{du}{dy}\right)_{y=0} = 0 \tag{1}$$

A positive C_f values indicate that the boundary layer remains attached to the surface. As the flow approaches the intersection point ($\xi = 0$), C_f drops and reaches zero, signaling the onset of separation. The negative C_f values observed over a range of positions indicate the presence and size of the separation bubble. The plot above 13 illustrates the linear relationship between the separation/reattachment points and the ramp angle. As the ramp angle is increased, the separation occurs earlier and the reattachment is delayed. The distance between the point of separation and reattachment indicate the size of separation bubble. Larger separation bubbles, associated with higher ramp angles, can result in increased drag and other aerodynamic penalties, making them critical considerations in high-speed aerodynamic design. Early separation at higher ramp angles can lead to more extensive and more unstable separation bubbles, negatively impacting the flow's overall stability and efficiency over the ramp.



(a) Separation point vs β (b) Reattachment point vs β

Figure 13 – Relationship between separation/reattachment point and ramp angles

3.1.3 Expansion fan

The expansion wave originating from a sharp convex corner is referred to as a centred expansion wave, commonly known as the Prandtl-Meyer wave. Since the entropy change is zero for each of

these Mach waves, the expansion is isentropic. A similar Prandtl-Meyer wave was observed at the trailing edge of the compression ramp within this domain 10. As the ramp angle (β) increases, the reflected shock (originating from the top wall) interacts with these expansion waves, resulting in an abrupt change in flow properties. The table shows that the error percentage becomes significantly higher at larger angles.

Table 6 – Flow properties at station 3 (expansion waves)

beta	Analytical solution		Simulation results		Error %	
(deg)	P_3 (Pa)	M_3	P_3 (Pa)	M_3	P_3	M_3
6	5891.3	2.50	6392.5	2.45	8.50	2.13
9	5911.6	2.49	6466.0	2.43	9.08	2.49
12	5965.8	2.47	6507.5	2.41	9.08	2.32
15	5954.8	2.45	6658.7	2.38	11.82	3.04
18	6053.1	2.41	6717.5	2.36	10.98	2.10
21	6178.3	2.36	7109.8	2.21	15.08	6.58

3.1.4 Separation near the top wall surface

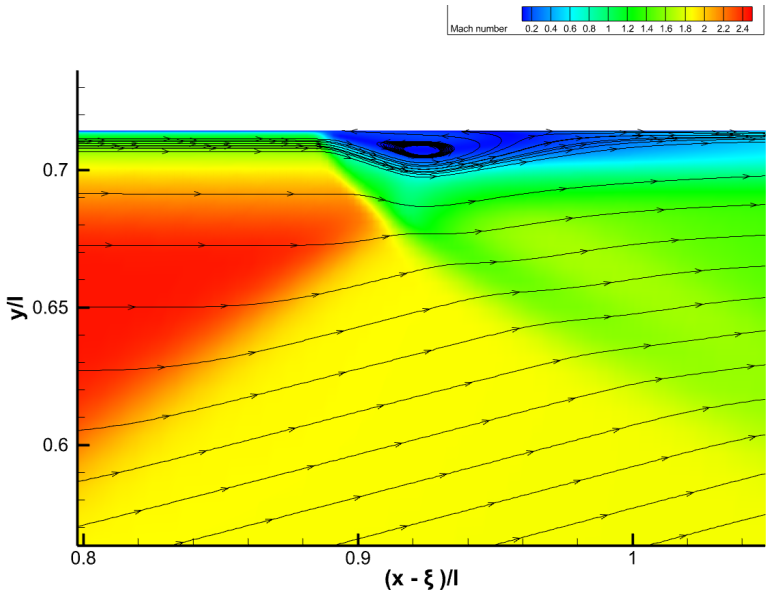


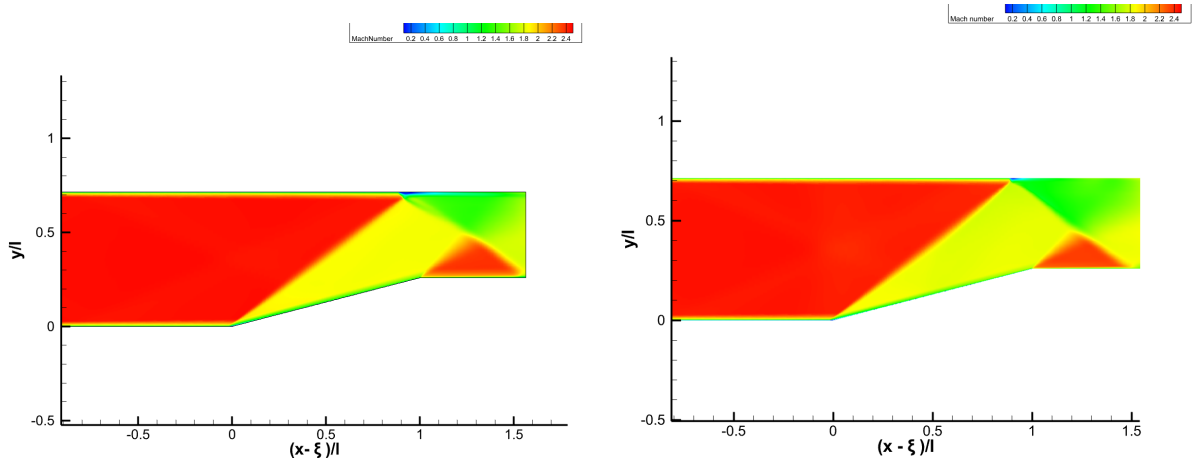
Figure 14 – Separation at top wall in the 2D domain at 15°

It was also observed that flow separation occurred near the top surface due to the reflected shock generated by the wall. As the ramp angle (β) increased, the shock angle (θ) also increased, causing the reflected shock to move forward, thereby enlarging the separation region on the top surface. When testing at a 24° ramp angle, it was noted that the separation interacted with the oblique shock, transforming it into a normal shock. Consequently, testing was halted at a 21° ramp angle to avoid further complications.

3.2 3D results

The plane at z=0 was sliced, and the flow properties across the separation shock were compared with the 2D results. From Figure 15, it is evident that the flow patterns in 2D and 3D are similar, indicating that 2D CFD is capable of predicting 3D flow in a narrow wind tunnel. The 3D post-oblique shock (separation shock) properties obtained at the $z = 0$ plane closely align with the 2D results, demonstrating good agreement between the two simulations.

The 2D analysis exhibited a 7.47% error compared to the 3D results without mesh adaptation (20 million cells) and a 3.17% error compared to the 3D results with mesh adaptation (38 million cells).



(a) 2D simulation results (b) 3D simulation results (z = 0 plane)

Figure 15 – Mach contour from 2D and 3D simulation for β = 15 $^\circ$

Table 7 – Comparison of 2D with 3D flow properties across separation shock

β ($^\circ$)	2D simulation		3D simulation (z = 0)		Error %	
	P_2 (Pa)	M_2	P_2 (Pa)	M_2	P_2	M_2
9	10835.6	2.10	11645.1	2.05	7.470	2.57
12	12753.4	1.98	13816.6	1.93	8.34	2.88
15	14909.8	1.863	16096.4	1.81	7.96	2.81
18	17410.6	1.738	18480.4	1.70	6.14	2.28
21	19933.7	1.624	21599.1	1.55	8.36	4.74

These findings indicate that 2D analysis can predict the 3D flow in a narrow wind tunnel model with much closer prediction values.

Table 8 – Comparison of flow properties across separation shock at β = 9°

Data	**Pressure (Pa)**	**Mach**
Theoretical	10425.501	2.127
2D simulation	10835.654	2.101
3D simulation (without mesh adaption)	11645.122	2.047
3D simulation (with mesh adaption)	11179.515	2.082

4. Conclusion

The study indicates that the ramp angle plays a critical role in determining the behavior of the flow, particularly affecting the size and location of separation bubbles, as well as the strength and positioning of shockwaves. The analysis revealed a linear relationship between ramp angles and separation/reattachment points, with higher ramp angles leading to more pronounced separation regions and stronger shock interactions. These phenomena significantly influence pressure distribution and flow stability, which are crucial considerations for high-speed aerodynamic design. Validation against theoretical solutions and the comparison between 2D and 3D simulations demonstrated that 2D analyses can provide accurate predictions for narrow wind tunnel scenarios. However, increasing the ramp angle beyond 21°resulted in significant complexities, including potential transitions to normal shocks, which may compromise stability and complicate modeling efforts. If experimental data for Mach 2.5 becomes available, it would be highly valuable to compare it with the current simulation

results. Such comparisons would provide an opportunity to verify the accuracy of the computational fluid dynamics (CFD) predictions and refine the model where necessary. This research underscores the importance of accurately capturing SWBLI dynamics for optimizing aerodynamic designs. Future studies may explore advanced three-dimensional configurations, higher Mach regimes, or alternative turbulence models to expand the applicability of these findings across diverse aerospace applications.

5. Contact Author Email Address

The contact author is Dr. Zeeshan A. Rana: zrana@pmu.edu.sa

6. Copyright Statement

The authors confirm that they, and/or their company or organization, hold copyright on all of the original material included in this paper. The authors also confirm that they have obtained permission, from the copyright holder of any third party material included in this paper, to publish it as part of their paper. The authors confirm that they give permission, or have obtained permission from the copyright holder of this paper, for the publication and distribution of this paper as part of the ICAS proceedings or as individual off-prints from the proceedings.

References

[1] Holger. Babinsky. Shock wave-boundary-layer interactions. 2011. Publisher: Cambridge University Press.

[2] D. W. Kuntz, V. A. Amatucci, and A. L. Addy. Turbulent boundary-layer properties downstream of the shock-wave/boundary-layer interaction. *AIAA Journal*, 25(5):668–675, May 1987.

[3] Zhengzhong Sun, Tian Gan, and Yun Wu. Shock-wave/boundary-layer interactions at compression ramps studied by high-speed schlieren. *AIAA Journal*, 58:1681–1688, 2020.

[4] Jean M. Delery. Shock wave/turbulent boundary layer interaction and its control. *Progress in Aerospace Sciences*, 22(4):209–280, January 1985.

[5] H. Babinsky and J. A. Edwards. On the incipient separation of a turbulent hypersonic boundary layer. *The Aeronautical Journal*, 100(996):209–214, July 1996.

[6] Frank K. Lu. New Results on the Incipient Separation of Shock/Boundary-layer Interactions. *Procedia Engineering*, 126:12–15, January 2015.

[7] Gary S. Settles, Seymour M. Bogdonoff, and Irwin E. Vas. Incipient Separation of a Supersonic Turbulent Boundary Layer at High Reynolds Numbers. *AIAA Journal*, 14(1):50–56, January 1976.

[8] Donald M. Kuehn. Experimental Investigation of the Pressure Rise Required for the Incipient Separation of Turbulent Boundary Layers in Two-Dimensional Supersonic Flow. Technical Report A-120, February 1959. NTRS Author Affiliations: NASA Ames Research Center NTRS Document ID: 19980230682 NTRS Research Center: Headquarters (HQ).

[9] Kshitij Sabnis and Holger Babinsky. A review of three-dimensional shock wave–boundary-layer interactions. *Progress in Aerospace Sciences*, 143:100953, November 2023.

[10] R. J. Stalker. Sweepback Effects in Turbulent Boundary-Layer Shock-Wave Interaction. *Journal of the Aerospace Sciences*, 27(5):348–356, May 1960.

[11] Gary Settles and David Dolling. Swept Shock Wave/Boundary-Layer Interactions (Review). pages 297–379. September 1986.

[12] Alexander J. Smits and Seymour M. Bogdonoff. A “Preview” of Three-Dimensional Shock-Wave/ Turbulent Boundary-Layer Interactions. In J. Délery, editor, *Turbulent Shear-Layer/Shock-Wave Interactions*, pages 191–202, Berlin, Heidelberg, 1986. Springer.

[13] Argyris G. Panaras. Review of the physics of swept-shock/boundary layer interactions. *Progress in Aerospace Sciences*, 32(2-3):173–244, 1996.

[14] A.A. Zheltovodov and D.D. Knight. Ideal-gas shock wave-turbulent boundary-layer interactions in supersonic flows and their modeling: Three-dimensional interactions. In *Shock Wave-Boundary-Layer Interactions*, pages 202–258. 2011.

[15] Zhengzhong Sun, Tian Gan, and Yun Wu. Shock-Wave/Boundary-Layer Interactions at Compression Ramps Studied by High-Speed Schlieren. *AIAA Journal*, 58(4):1681–1688, April 2020.

[16] Asmelash Haftu Amaha. Numerical investigation of shock wave turbulent boundary layer interaction over a 2d compression ramp, 2014.

[17] Noel T. Clemens and Venkateswaran Narayanaswamy. Low-frequency unsteadiness of shock wave/turbulent boundary layer interactions. *Annual Review of Fluid Mechanics*, 46:469–492, 1 2014.

[18] Kin Choong Muck, Jannis Andreopoulos, and Jean Paul Dussauge. Unsteady nature of shock-wave/turbulent boundary-layer interaction. *AIAA Journal*, 26:179–187, 1988.

[19] Rafael F. Vieira and João Luiz F. Azevedo. Rans simulations of flows with shock wave-boundary layer interaction. American Institute of Aeronautics and Astronautics Inc., 2013.

[20] Datta V. Gaitonde. Progress in shock wave/boundary layer interactions. *Progress in Aerospace Sciences*, 72:80–99, January 2015.

[21] Dennis M. Bushnell and Leonard M. Weinstein. Correlation of peak heating for reattachment of separated flows. *Journal of Spacecraft and Rockets*, 5(9):1111–1112, September 1968. Publisher: American Institute of Aeronautics and Astronautics.

[22] Jean Délery and Jean-Paul Dussauge. Some physical aspects of shock wave/boundary layer interactions. *Shock Waves*, 19(6):453–468, December 2009.

[23] James R Forsythe, Klaus A Hoflmannf, and Henri-Marie Damevin. An assessment of several turbulence models for supersonic compression ramp flow, 1998.